

Synthesis, crystal structure, vibrational spectral and density functional studies of 4-(1,3-dioxoisindolin-2-yl)antipyrene

Zongxue Yu^{a,d}, Gang Sun^{c,d}, Zengwei Liu^c, Cheng Yu^c, Changliang Huang^c, Yuxi Sun^{b,c,d,*}

^aSchool of Chemistry & Chemical Engineering, Southwest Petroleum University, Chengdu 610500, PR China

^bResearch Center of New Energy & Materials, Mianyang Normal University, Mianyang 621000, PR China

^cSchool of Chemistry and Chemical Engineering, Qufu Normal University, Qufu 273165, PR China

^dKey Laboratory of Education Ministry for Soft Chemistry and Functional Materials, Nanjing University of Science and Technology, Nanjing 210094, PR China

ARTICLE INFO

Article history:

Received 30 January 2012

Received in revised form 10 March 2012

Accepted 11 March 2012

Available online 26 March 2012

Keywords:

4-(1,3-Dioxoisindolin-2-yl)antipyrene

Synthesis

Crystal structure

Vibrational spectra

B3LYP calculations

ABSTRACT

The 4-(1,3-dioxoisindolin-2-yl)antipyrene, C₁₉H₁₅N₃O₃, was synthesized by the condensation reaction of 4-aminoantipyrene and phthalic anhydride in ethanol solution using triethylamine as catalyst, and characterized by X-ray diffraction and spectral techniques. The experimental spectral bands were structurally assigned with the theoretical calculation, and the thermodynamic properties of the studied compound were obtained from the theoretically calculated frequencies. The linear polarizability (α_0) and first hyperpolarizabilities (β_0) calculated at B3LYP/6-31G(d) level are of 33.6921 Å³ and 2.7835×10^{-30} cm⁵/esu, respectively. The NBO analysis reveals that the studied molecule presents a structural characteristic of long-range electron-transfer with the energy gap of ≥ 3.639 eV. The frontier molecular orbitals are responsible for the electron polarization and long-range electron-transfer properties. The results indicate that the compound might be an excellent candidate of photo-responsive materials.

© 2012 Elsevier B.V. All rights reserved.

1. Introduction

Following with the discovery of the antipyrene (AP) in 1883 [1], antipyrene derivatives (APDs) have been widely used in the biological and pharmaceutical fields because of their broad bioactivities of antitumor [2–4], antimicrobial [5–7], antiviral [8,9], and analgesics [10], so that APDs have been well accepted as one class of model compounds in many fields. Recently, an interest has been focused on organic compounds for functional materials in communications, signal processing, optical interconnection, etc. [11,12], and then the APDs are researched and their potential applications such as nonlinear optical and photovoltaic properties have been reported [13–15]. These successful examples prompt us to synthesize new APDs artificially and to study their photo-responsive properties in our work.

With the rapid development of computer techniques and computational chemistry, the quantum chemical techniques provide a good insight into molecular structure and propel the traditional chemistry development strongly [16]. A suitable quantum chemical study often contributes to a good insight for some experiments

or a suitable prediction for some potential materials. Currently, the density functional theory (DFT) method has become an efficient and accurate method in evaluating a number of molecular properties demonstrated by *ab initio* community among the theoretical calculations [17]. Nowadays, the DFT has been accepted as a popular post-HF approach to predict the structural characteristics, vibrational frequencies, functional predictions and so on [18].

In our previous work, we have reported some imine-bridged phenyl compounds with good nonlinear optical properties [19–24], which are tightly related to their imine-bridged π -conjugated substructures with nearly coplanar dihedral angle of less than 11.2(3)° between the pyrazoline and aromatic rings in each compounds reported previously [21,23,25–36]. Recently, we reported the structure and photoresponsive properties of 4-(2,5-dioxo-2H-pyrrol-1(5H)-yl)antipyrene (DOPYAP) with an obvious dihedral angle between pyrazoline and dioxopyrrole moieties [37], which presents a long-range electron transfer property with the energy gap of 3.895 eV. Enlightened by these previous works, we continue to chose 4-(1,3-dioxoisindolin-2-yl)antipyrene (DOIYAP) with obvious dihedral angle between pyrazoline and isoindoline-1,3-dione to aim its structural characteristics and photo-responsive properties in this work. Compared with DOPYAP, DOIYAP has one more benzene ring, which is in the hopes of better properties. The structure, vibrational spectra, thermodynamics, charge population, nonlinear optical and electron transfer properties were investigated in details for the studied compound.

* Corresponding author at: Research Center of New Energy & Materials, Mianyang Normal University, Mianyang 621000, PR China. Tel.: +86 816 2200064; fax: +86 816 2200819.

E-mail address: yuxisun@163.com (Y. Sun).

2. Experimental and theoretical methods

2.1. Experimental

2.1.1. Synthetic procedure

All the chemicals (reagent grade) were purchased from commercial sources and used without further purification.

The studied compound was prepared according to the procedure stated previously [6,37]. A mixture of 4-aminoantipyrine (1016.2 mg, 5 mmol) and phthalic anhydride (740.6 mg, 5 mmol) was dissolved in ethanol (35 mL) with stirring for 15 min at ice-bath cooling temperature, and then triethylamine (5 mL) as catalyst was added dropwise to the mixture. The reaction mixture was heated at reflux with magnetic stirring until the reactants were vanished (TLC monitoring). Then, the resulting solution was concentrated by distillation under reduced pressure, and the crude product was purified by silica gel column chromatography with acetone as eluent, and the target compound was recrystallized by evaporating ethanol solvent slowly at room temperature to gain the colorless plane-shaped crystals with yield 61%. The synthesis pathway of the title compound is shown in Scheme 1.

2.1.2. Spectral measurements

The FT-IR spectrum of the studied compound was recorded in the region of 4000–400 cm^{-1} in evacuation mode on a Bruker IFS 66 V FI-IR spectrometer with a scanning speed of 30 $\text{cm}^{-1} \text{min}^{-1}$ and a spectral width of 2.0 cm^{-1} using a KBr disc technique.

The FT-Raman spectrum of the solid sample was measured in the region 4000–100 cm^{-1} with a spectral resolution of 1.0 cm^{-1} in the backscattering configuration on a RENISHAW in Via Raman microscope with a counter current detector and a 785 nm diode laser excitation.

2.1.3. Crystal structure determination

The crystal structure of the studied compound was measured according to the following procedure. A single crystal ($0.15 \times 0.14 \times 0.04 \text{ mm}^3$) of DOIYAP was attached to a glass fiber. Data were collected with a ω - ϕ scan mode at 295(2) K on a Bruker AXS SMART APEX area-detector diffractometer (Mo K α radiation, $\lambda = 0.71073 \text{ \AA}$) with SMART [38] as driving software; data integration was performed with SAINT-Plus [39] and multiscan absorption correction was applied with using SADABS [40]. The non-H atoms of the crystal structure were obtained by solving and refining the Fourier differences and least squares of F^2 with anisotropic displacement parameters. All the H atoms attached to C were placed in calculated positions [aromatic C–H = 0.93 \AA and with $U_{iso}(\text{H}) = 1.2 U_{eq}(\text{C})$, methyl C–H = 0.96 \AA and with $U_{iso}(\text{H}) = 1.5 U_{eq}(\text{C})$]. All the calculations to solve the structure, to refine the model proposed, and to obtain derived result were carried out with the computer programs SHELXS-97 and SHELX-L97 [41] and SHELXTL [42]. Full use of the CCDC package was also made for searching

in CSD database. The crystallographic data and experimental details for the structural analyses were summarized in Table 1.

2.2. Theoretical

In this work, the quantum chemical calculations are used to make spectral assignments for DOIYAP based on the fundamental normal mode analysis, and to clarify experimentally recorded bands of FT-IR and FT-Raman spectra for the studied compound. Furthermore, the thermodynamic, nonlinear optical and electron transfer properties for the studied compound are obtained by other calculations based on the optimized structure.

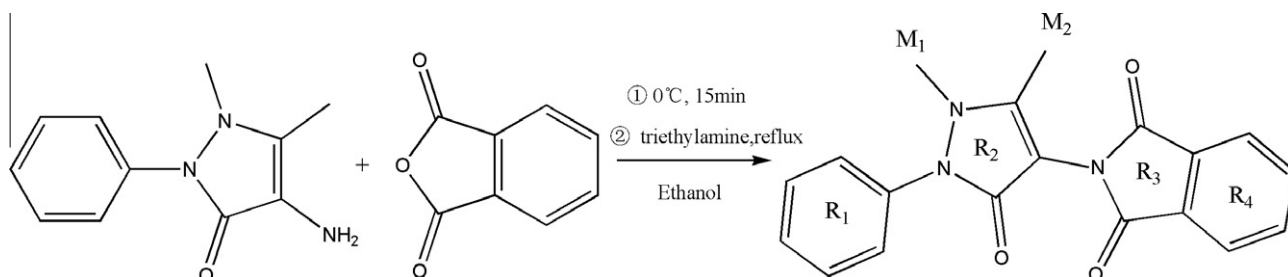
2.2.1. Calculation method and basis set

For meeting the requirements of accuracy and economy, the theoretical method and basis set are considered firstly. Calculations related to the density functional theory (DFT) have proved that the Becke's three-parameter hybrid method with the Lee, Yang and Parr correlation functional methods (B3LYP) is a very successful method in studying molecular structures. The basis set of 6-31G(d) has been used as a very effective and economical level for large organic molecules [43]. Based on the viewpoints, the DFT-

Table 1
Crystal data and X-ray experimental details for DOIYAP.^a

Empirical formula	C ₁₉ H ₁₅ N ₃ O ₃
Formula weight	333.34
Temperature	295(2) K
Wavelength	0.71073 \AA
Crystal system	Monoclinic
Space group	$P2_1/c$
Unit cell dimensions	$a = 13.952(2) \text{ \AA}$ $b = 15.935(2) \text{ \AA}$ $c = 7.349(1) \text{ \AA}$ $\beta = 102.409(2)^\circ$
Volume (Z)	1595.6(4) \AA^3 , 4
Density (calculated)	1.388 Mg m^{-3}
Absorption coefficient	0.096 mm^{-1}
$F(000)$	696
Crystal size	0.15 \times 0.14 \times 0.04 mm^3
θ Range for data collection	2.6–26.3°
Limiting indices	$-17 \leq h \leq 17$ $-19 \leq k \leq 20$ $-9 \leq l \leq 9$
Reflections collected/unique	12324/3287 [$R_{int} = 0.04$]
Absorption correction	Multi-scan
Max. and min. transmission	0.996 and 0.986
Refinement method	F^2
Goodness-of-fit on F^2	1.12
Final R indices [$I > 2\sigma(I)$]	$R_1 = 0.0592$ $wR_2 = 0.1270$
R indices (all data)	$R_1 = 0.0846$ $wR_2 = 0.1370$
Extinction coefficient	None
Largest diff. peak and hole	0.26 and -0.19
CCDC	835063

^a $R_1 = \sum ||F_o| - |F_c|| / \sum |F_o|$, $wR_2 = (\sum w(F_o^2 - F_c^2)^2 / \sum w(F_o^2)^2)^{1/2}$, where $w\sigma = 1 / [2(F_\sigma^2) + (0.0166(F_\sigma^2 + 2F_\sigma^2))^2 + 0.2155(F_\sigma^2 + 2F_\sigma^2)]$.



Scheme 1. The synthesis pathway of DOIYAP.

B3LYP at 6-31G(d) basis set level was adopted to calculate the molecular properties for the present compound in this work. All the calculations were performed using Gaussian 03W program package [44] with the default convergence criteria.

2.2.2. Optimization procedure

For the investigated molecule, the initial geometrical configuration was generated from its X-ray diffraction (XRD) crystallographic data, and the optimized geometry corresponding to the minimum potential energy surface was obtained by solving self-consistent field equation iteratively without any constraints. The harmonic vibrational frequencies were analytically calculated by taking the second order derivative of energy using the same level of theory. Normal coordinate analysis was performed to obtain full description of the molecular motion pertaining to the normal modes using the GaussView program [45]. Simultaneously, the statistical thermodynamic functions were theoretically predicted by the harmonic frequencies of the optimized structures for the title compound.

2.2.3. Theoretical Raman intensity

According to the basic theory of Raman stated in previous works [46,47], the relative Raman intensities can be obtained from the Raman scattering activities by using the following relationship.

$$I_i = \frac{f(\nu_0 - \nu_i)^4 S_i}{\nu_i \left[1 - \exp\left(\frac{-h\nu_i}{kT}\right) \right]} \quad (1)$$

where ν_0 is the exciting frequency (in cm^{-1} units); ν_i is the vibrational wavenumber of the i th normal mode; h , c and k are universal constants, and f is the suitably chosen common scaling factor for all the peak intensities.

2.2.4. Nonlinear optical calculation

The nonlinear optical (NLO) materials have a wide range of applications in the communications, data storage, optical signal processing. And the nonlinear optical property is associated with molecular nonlinear polarization.

For a molecule, the non-linear polarization (p) can be expressed as follows.

$$p = \mu_0 + \alpha_{ij}E_j + \beta_{ijk}E_jE_k + \gamma_{ijkl}E_jE_kE_l + \dots \quad (2)$$

where μ_0 is the molecular dipole moment, α_{ij} is the linear polarizability, β_{ijk} is the first-order hyperpolarizability and γ_{ijkl} is the second-order hyperpolarizability. The subscripts i , j , k and l denotes the x , y and z axes determined arbitrarily.

The NLO-related properties can be obtained by the theoretical methods stated previously [48–58]. The total static dipole moment (μ_0), polarizability (α_0) and first-order hyperpolarizability (β_0) using the x , y , z components are defined as:

$$\mu_0 = \sqrt{\mu_x^2 + \mu_y^2 + \mu_z^2} \quad (3)$$

$$\alpha_0 = \frac{\alpha_{xx} + \alpha_{yy} + \alpha_{zz}}{3} \quad (4)$$

$$\beta_0 = \sqrt{(\beta_{xxx} + \beta_{xyy} + \beta_{xzz})^2 + (\beta_{yyy} + \beta_{xxy} + \beta_{yzz})^2 + (\beta_{zzz} + \beta_{xxz} + \beta_{yyz})^2} \quad (5)$$

2.2.5. Natural bond orbital calculation

According to the natural bond orbital (NBO) basis of donor-acceptor viewpoint [59], the interorbital interactions result in a loss of occupancy from the localized NBO of the idealized Lewis structure into an empty non-Lewis orbital. The energy of these

interactions can be estimated by the second order perturbation theory. For each donor (i) and acceptor (j), the stabilized energy $E^{(2)}$ associated with the delocalization $i \rightarrow j$ can be estimated as follows:

$$E_{ij}^{(2)} = \Delta E_{ij} = q_i \frac{F_{ij}^2}{\varepsilon_j - \varepsilon_i} = q_i \frac{F_{ij}^2}{\Delta \varepsilon_{ij}} \quad (6)$$

wherein, q_i is the i th donor orbital occupancy, ε_i and ε_j are diagonal elements, $\Delta \varepsilon_{ij}$ is energy gap between donor (i) and acceptor (j) NBO orbitals, and F_{ij} is the off diagonal NBO FOCK matrix element. A useful aspect of the NBO method is that it gives information about interactions in both filled and virtual orbital spaces, which can be used to accurately evaluate the donor-acceptor interactions [17,60].

3. Results and discussion

3.1. Crystal structure

The displacement ellipsoid plot of DOIYAP with the atom numbering is shown in Fig. 1, and the atomic coordinates and thermal parameters can be obtained from the Supplementary materials. Selected bond lengths and bond angles obtained by X-ray diffractions (XRDs) are listed in Table 2 along with the calculated parameters.

As shown in Table 2, the bond distances of O1–C7, O2–C12 and O3–C15 are 1.223(3) Å, 1.198(3) Å and 1.202(3) Å, respectively. The relatively short C–O bond distances are consistent with the presence of ketones with double bonds. The N3–C8 bond length [1.417(3) Å] is longer than those of previously reported compounds [19–24], which implies that there are no conjugated effects between the present pyrazoline and isoindoline rings. The N1–C1 bond length [1.419(3) Å], however, is close to the value of the classical C–N single bond [1.44 Å]. Thus, three conjugated moieties, viz., phenyl ring, pyrazolone and dioxoisindoline, could be separated from the studied molecule as expected, which may be more helpful to form an effective charge transfer barrier.

The phenyl group exhibits normal bond lengths as observed in benzene. In the pyrazolone ring, however, all atoms are almost coplanar with a mean deviation of 0.047(3) Å, and the directly linked methyl groups of C10 and C11 are the same side of the pyrazolone plane with respective distances of 0.043(3) Å and 0.743(3) Å. In dioxoisindoline, the N3–C12 and N3–C15 bond lengths are of 1.413(3) Å and 1.408(3) Å, respectively, which are slightly lower than that of the classical C–N single bond [1.44 Å], and the similar phenomenon also observed in the bond distances of C12–C13 and C14–C15, which are relatively lower values of 1.486(3) Å and 1.485(3) Å than the normal C–C single bond. Significantly, the No. 4 ring shows normal bond lengths of benzene ring, which indicates that the dioxoisindoline presents an excellent conjugative structure with mean planar deviation of 0.015(2) Å.

As expected, the three moieties form effective dihedral angles each other. The phenyl and pyrazoline rings form an effective dihe-

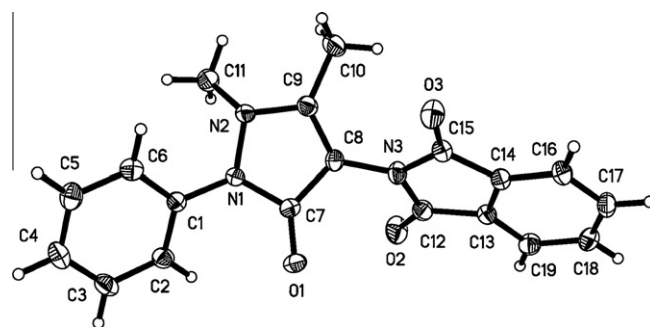


Fig. 1. The schematic diagram with atomic numbering for DOIYAP.

Table 2
Selected geometric parameters for DOIYAP.

Parameters	Exp.	Calc.	Parameters	Exp.	Calc.
<i>Bond lengths (Å)</i>					
N1–N2	1.411(2)	1.416	C3–C4	1.377(4)	1.396
N1–C1	1.419(3)	1.421	C4–C5	1.374(4)	1.395
N1–C7	1.395(3)	1.417	C5–C6	1.382(3)	1.394
N2–C9	1.382(3)	1.391	C7–C8	1.437(3)	1.461
N2–C11	1.471(3)	1.469	C8–C9	1.345(3)	1.358
N3–C8	1.417(3)	1.405	C9–C10	1.482(3)	1.493
N3–C12	1.413(3)	1.416	C12–C13	1.486(3)	1.490
N3–C15	1.408(3)	1.419	C13–C14	1.382(3)	1.395
O1–C7	1.223(3)	1.219	C14–C15	1.485(3)	1.491
O2–C12	1.198(3)	1.209	C14–C16	1.374(3)	1.387
O3–C15	1.202(3)	1.212	C16–C17	1.383(3)	1.401
C1–C2	1.382(3)	1.401	C17–C18	1.382(3)	1.401
C1–C6	1.384(3)	1.401	C18–C19	1.387(3)	1.401
C2–C3	1.378(3)	1.393	C13–C19	1.375(3)	1.387
<i>Bond angles (°)</i>					
N2–N1–C1	120.4(2)	118.9	N3–C8–C9	127.7(2)	127.9
N2–N1–C7	109.8(2)	109.8	C7–C8–C9	110.0(2)	109.4
C1–N1–C7	124.5(2)	123.6	N2–C9–C8	109.4(2)	109.9
N1–N2–C9	106.1(2)	106.6	N2–C9–C10	120.8(2)	120.8
N1–N2–C11	114.5(2)	113.8	C8–C9–C10	129.7(2)	129.3
C9–N2–C11	119.5(2)	118.5	N3–C15–O3	125.1(2)	125.4
C8–N3–C15	125.4(2)	123.1	N3–C15–C14	105.5(2)	105.3
C8–N3–C12	122.6(2)	124.3	O3–C15–C14	129.4(2)	129.2
C15–N3–C12	111.8(2)	111.9	C15–C14–C13	108.6(2)	108.6
N1–C1–C2	118.2(2)	118.6	C15–C14–C16	130.0(2)	129.8
N1–C1–C6	121.9(2)	121.1	C13–C14–C16	121.4(2)	121.48
C2–C1–C6	119.9(2)	120.1	C14–C13–C12	108.8(2)	108.6
C1–C2–C3	119.7(2)	119.4	C14–C13–C19	121.4(2)	121.5
C2–C3–C4	120.6(2)	120.7	C12–C13–C19	129.7(2)	129.8
C3–C4–C5	119.5(2)	119.4	N3–C12–O2	124.9(2)	125.5
C4–C5–C6	120.7(2)	120.4	N3–C12–C13	105.1(2)	105.4
C1–C6–C5	119.5(2)	119.6	O2–C12–C13	130.0(2)	129.1
N1–C7–O1	124.9(2)	125.6	C13–C19–C18	117.3(2)	117.4
N1–C7–C8	103.7(2)	103.7	C19–C18–C17	121.3(2)	121.1
O1–C7–C8	131.3(2)	130.6	C18–C17–C16	120.9(2)	121.1
N3–C8–C7	122.2(2)	122.4	C14–C16–C17	117.7(2)	117.4

dral angle of $36.6(2)^\circ$, resembling to previously reported compounds [21,23,25–36]. The dioxoisindoline moiety forms a dihedral angle of $57.0(2)^\circ$ with pyrazoline moiety due to the steric hindrance from two keto groups of dioxoisindoline, which is obviously different from the previously reported compounds [21,23,25–36].

Intermolecular interactions can be revealed by the packing structural analysis for neighboring molecules. There are three kinds of intermolecular weak hydrogen bonds in the molecule packing structure (Table 3). The adjacent molecules are linked through the three kinds of hydrogen bonding of $C4-H4 \cdots O3^i$ (i: $1-x, 1-y, 1-z$), $C10-H10C \cdots O1^{ii}$ (ii: $x, y, -1+z$) and $C19-H19 \cdots O1^{iii}$ (iii: $-x, 1-y, 1-z$), to form a network supermolecular architecture along with the *ac* plane as shown in Fig. 2a. Wherein, the bonding of $C4-H4 \cdots O3^i$ (i: $1-x, 1-y, 1-z$) and $C10-H10C \cdots O1^{ii}$ (ii: $x, y, -1+z$) make neighboring molecules propagating along the *a* axis, and the bonding of $C19-H19 \cdots O1^{iii}$ (iii: $-x, 1-y, 1-z$) make neighboring molecules propagating along the *b* axis. The molecular isoindoline moieties between adjacent layers, however, are almost parallel to each other (their di-

Table 3
Hydrogen-bond parameters for DOIYAP. ^a

	D–H (Å)	H···A (Å)	D···A (Å)	D–H···A (°)
$C4-H4 \cdots O3^i$	0.930	2.540	3.339 (3)	144.0
$C10-H10C \cdots O1^{ii}$	0.960	2.370	3.296 (3)	163.0
$C19-H19 \cdots O1^{iii}$	0.930	2.500	3.308 (3)	145.0

^a Symmetry codes: (i) $1-x, 1-y, 1-z$; (ii) $x, y, -1+z$; (iii) $-x, 1-y, 1-z$.

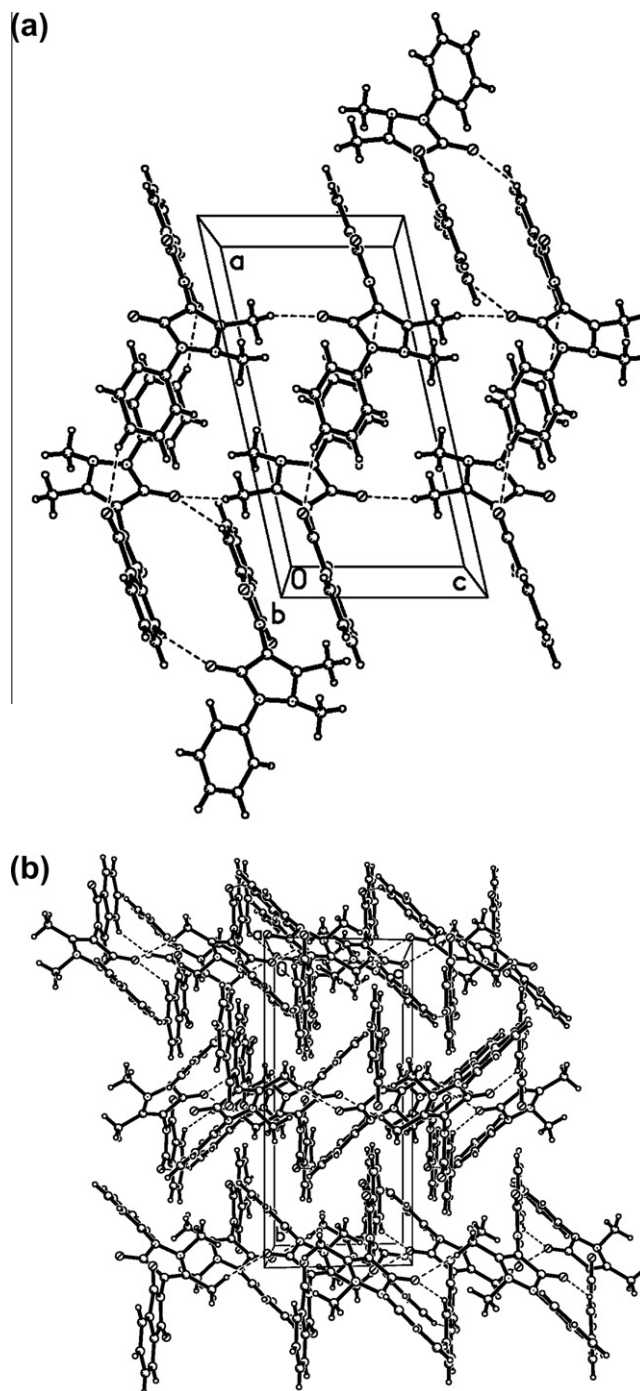


Fig. 2. The molecular packing diagrams of DOIYAP.

dral angle is of $3.2(2)^\circ$) with π – π interactions of $3.675(3) \text{ \AA}$, yielding a molecule-layer structure along the *b* axis (Fig. 2b). In addition, the neighboring intermolecular interaction pattern revealed by X-ray diffraction analysis gives an excellent interpretation for the plane-shape crystal characteristics of the studied compound.

3.2. Optimized structure

The first task is to determine the structure for a studied substance in a theoretical work since the theoretical results of material properties are decided by its structure. The initial geometrical configuration of the studied compound was taken from its X-ray crys-

tallographic data (Table 2), and was optimized by the Becke's three-parameter hybrid exchange and a Lee–Yang–Parr gradient-corrected correlation functional model at the 6-31G(d) level without any constraints. The harmonic vibrational frequencies were performed to convince that all normal vibrational modes are positive and the optimized structure is at a stable ground state. The optimized bond lengths and angles using B3LYP method with 6-31G(d) basis are listed in Table 2 for comparison with experimental data.

As seen from Table 2, most of the optimized bond lengths are longer than experimental ones agreeing within 0.024(3) Å, and the bond angles between the optimized and measured structures give the slight differences agreeing within 2.3(2)°. The structural discrepancy is due to the fact that the molecules in the theoretical and experimental methods are in the different states. The isolated molecule considered in theoretical calculation in gas phase is contrary to the packing molecules with intermolecular interactions recorded in condensed phase in the XRD measurement.

Although the theoretical geometric parameters of the optimized structure are not exactly close to the experimental ones for the studied compound, it is generally accepted that the optimized configuration obtained by the method and basis set used in the calculation represents a good approximation and can be used as a structural foundation to calculate the other properties of the compound.

3.3. Vibrational spectra

For the spectral description, the four rings and methyl groups of the studied molecule were labeled shown in Scheme 1. The studied molecule belongs to C₁ point group, and theoretically presents 114 normal vibrational modes for the 40-atom molecule.

Because of the electron correlation approximate treatment, as well as anharmonicity effects and basis set deficiencies, etc. [61,62], the results obtained by theoretical calculations are usually higher than their corresponding experimental ones. So, the theoretical harmonic frequencies obtained by B3LYP/6-31G(d) method were intentionally calibrated by the scaling factor of 0.9614 according to Refs. [63,64]. The recorded FT-IR and FT-Raman spectra are respectively shown in Figs. 3 and 4, where the infrared and

Raman intensities are plotted against the vibrational wavenumbers. For comparison, the theoretical IR and Raman spectra were simulated by using pure Lorentzian band shapes with a bandwidth of 8 cm⁻¹ and respectively inserted in Figs. 3 and 4 along with the corresponding experimental spectra.

In order to compare with the experimental FT-Raman, each of the theoretical Raman scattering activities (S_i) obtained by the B3LYP calculation was suitably converted to relative Raman intensities (I_i) according to Eq. (1). All the experimentally recorded absorption wavenumbers and theoretically calculated harmonic frequencies as well as their theoretical intensities and proposed vibrational assignments were summarized in Table 4.

3.3.1. Carbonyl vibrations

The carbonyl compounds usually present the infrared absorption and Raman scattering activities observed in the range of 1650–1800 cm⁻¹ [65]. It is a very difficult task to assign the experimental bands for carbonyl groups due to the large difference between the recorded and simulated IR spectra. Obviously, it is not easy to distinguish the stretching vibrational modes of carbonyl groups in the simulated IR spectrum, while there are five bands in the region of 1679–1783 cm⁻¹ in recorded FT-IR spectrum. The theoretical bands of 1789 and 1744 cm⁻¹ (mode Nos. 99, 98) are respectively ascribed to the symmetric and asymmetric stretching vibrations of carbonyl groups in the isoindoline substructure, and they cannot present the respective modes for C12–O2 and C15–O3, though the FT-IR feature shows four characteristic bands for them. According to the Hooke's law of elasticity and the solid structural parameters measured by XRD (Table 2), the recorded bands can be assigned clearly. The bands at 1783 and 1735 cm⁻¹ in FT-IR are ascribed to the C12–O2 stretching vibrational modes, and the bands of 1763 and 1717 cm⁻¹ in FT-IR are ascribed to the C15–O3 stretching modes. The C7–O1 vibrational mode presents the band recorded at 1679 cm⁻¹ and found at 1733 cm⁻¹ (mode No. 97), which is the same as the previously reported values for the similar compounds [19–24]. It is evident that the band of 1789 cm⁻¹ in FT-Raman spectrum is designated to the symmetric stretching vibrations of carbonyl groups in the isoindoline, which is in excellent agreements with the theoretical band (mode No. 99). The nodding vibrations of the C12–O2 and C15–O3 are

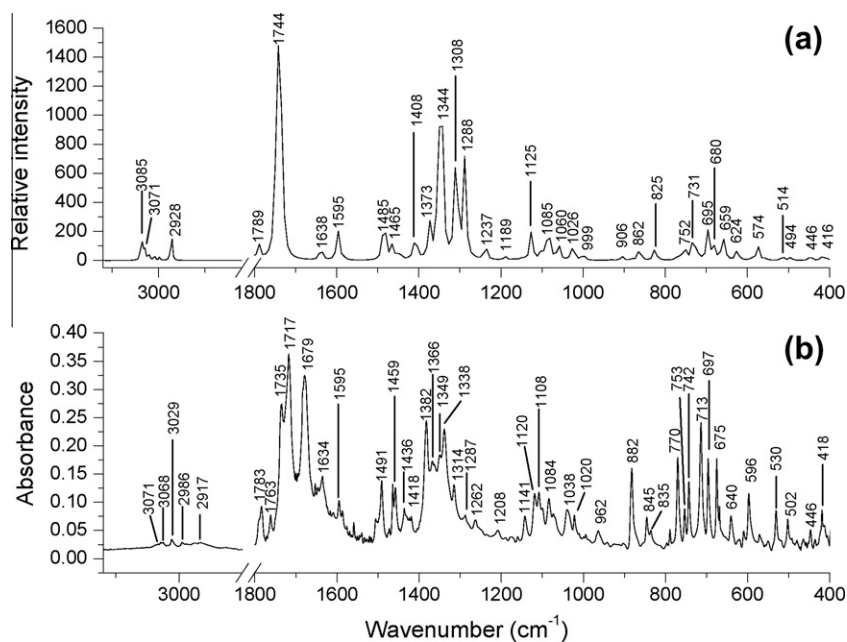


Fig. 3. IR spectra of the studied compounds: (a) simulated (b) recorded.

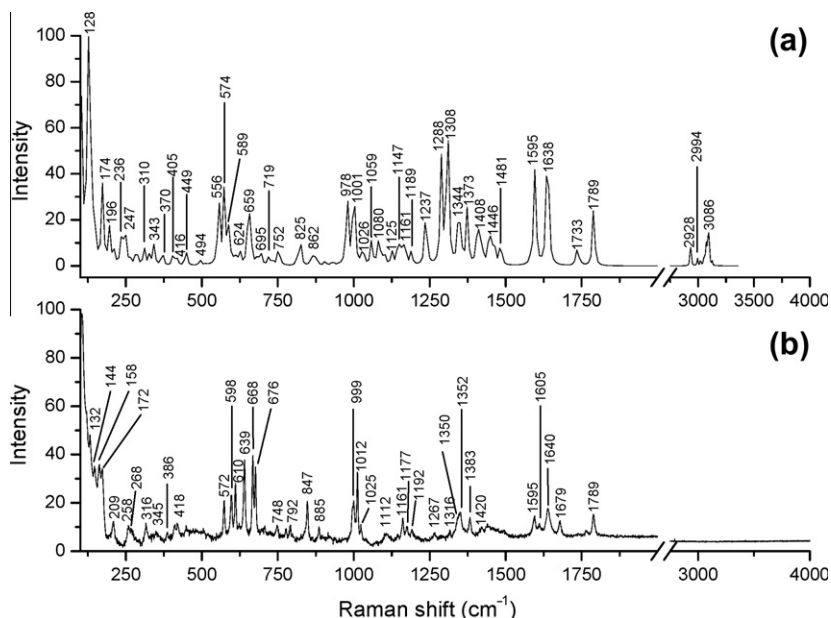


Fig. 4. Raman spectra of the studied compounds: (a) simulated (b) recorded.

presented by the weak band at 345 cm^{-1} in Raman spectra (mode No. 21).

3.3.2. Methyl vibrations

The studied molecule possesses two methyl groups labeled as M_1 and M_2 in the pyrazoline ring (Scheme 1). The weak bands observed at 2917 , 2986 , 3029 cm^{-1} in FT-IR are ascribed to the C–H stretching vibrations of methyl groups, which shows good agreements with the theoretical bands of 2928 , 2937 , 3022 cm^{-1} (mode Nos. 100, 101 and 103). The C–H scissoring deformations of methyl groups are expected in the region 1400 – 1485 cm^{-1} [66,67]. In the present study, the bands observed at 1464 and 1475 cm^{-1} are assigned to C–H scissoring vibrations, which show good agreements with the theoretical values of 1465 and 1481 cm^{-1} (mode Nos. 89, 90). The C–H umbrella vibrations for methyl groups usually appear in the range of 1360 – 1390 cm^{-1} [66,67]. In the present study, the weak bands observed at 1418 , 1382 cm^{-1} in FT-IR and 1420 , 1383 cm^{-1} in FT-Raman are assigned to the C–H umbrella deformation vibrations of M_1 and M_2 , which shows excellent agreements with the theoretical bands found at 1420 and 1373 cm^{-1} (mode Nos. 83, 81). The bands observed at 1141 , 1120 and 1038 cm^{-1} in FT-IR and 1025 cm^{-1} in FT-Raman are assigned to the methyl rocking vibrations, which are consistent with the theoretical results (mode Nos. 67, 66, 60). The middle intensity band recorded at 882 cm^{-1} in FT-IR is mainly designated to the rocking vibrations of the methyl groups partly mixed with the N_2 – C_9 stretching mode. The methyl nodding vibrations are observed at the bands of 316 , 209 , 132 cm^{-1} in FT-Raman partly along with the C_7O_1 , C_8 – N_3 -coupled nodding vibrations.

3.3.3. Phenyl and isoindoline vibrations

In the present study, the weak bands at 3071 and 3068 cm^{-1} in FT-IR are ascribed to the C–H stretching vibrations, corresponding to the theoretical results at 3072 and 3071 cm^{-1} (mode Nos. 110, 108). The weak bands at 1177 and 1161 cm^{-1} in FT-Raman are assigned to the C–H in-plane bending vibrations of benzene rings, corresponding to the theoretically computed bands of 1143 – 1169 cm^{-1} (mode Nos. 68, 69, 70, 71, 72). The band at 1287 cm^{-1} in FT-IR is ascribed to the C–H in-plane bending vibrations of No. 4 ring. The middle bands at 770 , 753 , 742 , 713 and 697 cm^{-1}

in FT-IR belong to the C–H out-of-plane bending vibrations, which are consistent with the theoretical bands found at mode Nos. 45, 43, 42, 40, 38. A weak band at 962 cm^{-1} in FT-IR ascribed to the C–H out-of-plane shows blue-shift of 29 cm^{-1} compared to the corresponding theoretical value (mode No. 53).

The bands observed at 1595 , 1366 , 1314 cm^{-1} in FT-IR and 1605 , 1595 , 1353 cm^{-1} in FT-Raman are assigned to the C=C stretching vibrations of benzene rings. The breathing vibration of No. 1 ring is observed at 999 cm^{-1} in FT-Raman. The band observed at 502 cm^{-1} in FT-IR is assigned to the puckering vibration, which is consistent with the theoretical value of 494 cm^{-1} (mode No. 28). The bands at 845 cm^{-1} in FT-IR and 885 cm^{-1} in FT-Raman are ascribed to the angle bending vibrational mode of No. rings 3, 4, corresponding to the theoretical value of 862 cm^{-1} (mode No. 48). The bands at 530 cm^{-1} in FT-IR and 572 cm^{-1} in FT-Raman are assigned to the angle bending vibrations of No. rings 3, 4. The wagging vibration of the dioxoisindoline is observed at 258 cm^{-1} in the FT-Raman spectrum, corresponding to the frequency of 236 cm^{-1} obtained by the theoretical calculation (mode No. 15). The nodding and torsion vibrations of the dioxoisindoline substructure are respectively presented at 172 (observed)/ 174 (found) cm^{-1} and 144 (observed)/ 136 (found) cm^{-1} in the Raman spectra.

The other bands related to aromatic rings are ascribed to the mixed vibrations. The band at 1491 cm^{-1} in FT-IR is ascribed to a mixed vibration of the C–H in-plane bending, C=C stretching and methyl scissoring modes, and the band at 1338 (recorded)/ 1308 (found) cm^{-1} in FT-IR belongs to the C=C stretching vibration of No. 4 benzene ring with the N_1 – C_7 stretching vibration. The bands at 1020 (recorded)/ 997 , 1001 (found) cm^{-1} in the IR spectra are designated to the breathing of No. 1 ring and angle bending with the C–H in-plane bending vibrations of No. 4 ring. The bands at 1084 (recorded)/ 1060 (found) cm^{-1} in the IR spectra are the angle bending vibration with the C–H in-plane bending of No. 4 ring. The bands at 1112 (recorded)/ 1080 (found) cm^{-1} in the Raman spectra are ascribed to the C–H in-plane bending of No. ring with the C_7 – N_1 stretching bending. The bands recorded at 835 cm^{-1} in FT-IR and 847 cm^{-1} in FT-Raman are ascribed to the angle bending vibration of phenyl ring with the C_7 – C_8 – N_3 angle bending mode. The middle intensity bands at 675 cm^{-1} in FT-IR and 676 cm^{-1} in FT-Raman are ascribed to the mixed vibration of the angle bending

Table 4

Comparison of the calculated and experimental vibrations of DOIYAP. ^a

Modes	Experimental			Theoretical		Approximate assignments
	IR	Raman	Freq.	I_{IR}	I_{Raman}	
9		132	128	1.0	29.5	$\eta M_1 + \eta M_2 + \eta C7O1$
10		144	136	0.1	48.1	$\tau R_{3,4}$
11		159	146	2.9	25.3	$\eta M_1 + \eta C7O1$
12		172	174	2.4	43.9	$\eta R_{3,4}$
13		209	196	3.0	20.5	ηM_2
15		258	236	0.7	15.9	$\omega R_{3,4}$
16		268	247	1.1	25.2	ηR_1
19		316	310	7.0	10.3	$\eta M_1 + \eta M_2 + \eta C7O1 + \eta C8N3$
21		345	343	15.2	12.4	$\eta C12O2 + \eta C15O3$
22		386	370	0.7	9.2	ρR_2
25	418	419	416	10.6	6.5	νR_2
26	446		446	9.3	2.8	νR_2
28	502		494	6.2	3.3	νR_1
29	530		514	8.4	0.8	$\alpha R_{3,4}$
30		572	556	3.8	44.5	$\alpha R_{3,4}$
31	596	598	574	29.9	51.1	νR_2
32		610	589	3.4	23.6	$\alpha R_1 + \alpha N2C9C8$
34	640	639	624	22.5	9.8	$\alpha R_1 + \alpha N1N2C9$
36		668	652	2.7	17.0	$\alpha R_1 + \tau R_2$
37	675	676	659	49.2	32.8	$\alpha R_4 + \tau R_2$
38	697		680	23.1	2.4	γCH of R_1
40	713		695	57.4	6.4	γCH of R_4
42	742		731	56.0	4.1	γCH of R_1
43	753	748	752	28.5	13.8	γCH of R_1
45	770		768	9.6	0.8	γCH of R_4
46		792	816	1.3	7.5	γCH of R_1
47	835	847	825	23.7	15.4	$\alpha R_1 + \alpha C7C8N3$
48	845	885	862	25.9	8.5	$\alpha R_{3,4}$
51	882		906	8.6	3.0	$\rho M_{1,2} + \nu N2C9$
53	962		933	0.8	1.3	γCH of R_4
56		999	978	0.1	54.9	θR_1
57	1020		997	6.2	12.7	$\theta R_1 + \alpha R_4 + \beta CH$ of R_4
58	1020	1012	1001	6.3	52.0	$\theta R_1 + \alpha R_4 + \beta CH$ of R_4
60	1038	1025	1026	18.6	6.1	$\rho M_{1,2}$
63	1084		1060	26.9	2.7	$\alpha R_4 + \beta CH$ of R_4
64		1112	1080	21	12.0	βCH of $R_1 + \nu C7N1$
65	1108		1085	52.3	10.7	$\nu C15N3$
66	1120		1100	23.8	10.8	ρM_1
67	1141		1125	58.9	9.7	ρM_1
69		1161	1147	0.4	6.1	βCH of R_1
71		1177	1161	0.3	15.1	βCH of R_1
73	1208	1192	1189	7.0	10.0	$\nu N1N2 + \rho M_1$
74	1262	1267	1237	30.8	46.3	$\nu C7N1 + \nu C8N3 + \nu C12C13 + \nu C14C15$
75	1287		1266	1.1	0.1	βCH of R_4
76	1314		1288	196.8	76.7	$\nu C=C$ of R_1
77	1338		1308	249.7	128.2	$\nu C=C$ of $R_1 + \nu N1C7$
79	1349	1350	1344	309.2	33.7	$\nu N2C9 + \nu N3C8 + \rho M_{1,2}$
80	1366	1352	1351	203.4	23.1	$\nu C=C$ of R_4
81	1382	1383	1373	68.3	43.2	ψM_2
83	1418	1420	1420	1.9	19.0	ψM_1
89	1436		1465	26.8	10.4	$\delta M_{1,2}$
90	1459		1481	30.3	9.0	δM_1
91	1491		1485	62.9	9.5	βCH of $R_1 + \nu C=C$ of $R_1 + \delta M_1$
93	1595	1595	1595	50.1	65.1	$\nu C=C$ of R_1
95		1605	1599	11.3	16.2	$\nu C=C$ of R_4
96	1634	1640	1638	27.2	131.3	$\nu C8C9$
97	1679	1679	1733	255.3	12.3	$\nu C7O1$
98	1717		1744	512.1	5.7	$\nu C12O2 + \nu C15O3$
	1735					
99	1763	1789	1789	30.8	50.6	$\nu C12O2 + \nu C15O3$
	1783					
100	2917		2928	46.9	12.2	νCH of M_1
101	2986		2937	18.6	26.4	νCH of M_2
103	3029		3022	11.8	8.3	νCH of M_1
108	3068		3072	17.3	14.1	νCH of R_1
110	3071		3086	35.4	21.0	νCH of R_1

^a Mode numbers are extracted from the output result of the B3LYP calculation. Observed wavenumbers (IR and Raman) and theoretical vibrational frequencies (Freq.) are in cm^{-1} ; the calculated IR intensities are in k mmol^{-1} ; the calculated Raman scattering intensities (I_{Raman}) are in arbitrary units by Eq. (1). R, ring; M, methyl; α , angle bending; β , in-plane bending; γ , out-of-plane bending; ω , wagging; ν , puckering; θ , breathing; δ , scissoring; ν , stretching; ρ , rocking; ψ , umbrella; η , nodding; τ , torsion.

of No. 4 ring and the torsion mode of No. 2 ring, while the same intensity band at 668(recorded)/652(found) cm^{-1} in the Raman

spectra is designated to the mixed vibration of the angle bending of No. 1 ring and the torsion mode of No. 2 ring.

3.3.4. Pyrazoline ring vibrations

The middle intensity bands at about 1634 cm^{-1} in FT-IR and 1640 cm^{-1} in FT-Raman are assigned to the C8–C9 stretching vibrations. The theoretical frequency at 1638 cm^{-1} (mode No. 96) computed by B3LYP method agree well with the experimentally recorded bands. The pyrazoline puckering vibrations occurred at $596, 446, 418\text{ cm}^{-1}$ in FT-IR, and the similar vibrational modes can be also observed in the FT-Raman spectrum of the compound.

With the exception of bands mentioned in Section 3.3.3, some other pyrazoline-related mixed vibrations also coexist because the pyrazoline substructure resides in the center position of the molecule. For example, the bands at 1349 cm^{-1} in FT-IR and 1350 cm^{-1} in FT-Raman are assigned to the N2–C9, C8–N3 stretching vibrations with the methyl rocking vibrations, while the bands at 1262 cm^{-1} in FT-IR and 1267 cm^{-1} in FT-Raman are designated to the mixed vibration of the C7–N1, C8–N3, C12–C13, C14–C15 stretching modes. Similarly, the bands appeared at $1208(\text{FT-IR})/1192(\text{FT-Raman})\text{ cm}^{-1}$ are ascribed to the N1–N2 stretching and methyl rocking vibrations, and the bands at 640 cm^{-1} in FT-IR and 639 cm^{-1} in FT-Raman are ascribed to the N1–N2–C9 and phenyl angle bending vibrations.

Obviously, the experimental and theoretical spectral analysis are supported each other on the whole and they reveal the molecular vibrational properties together.

3.4. Thermodynamic properties

Based on the statistical thermodynamics and vibrational frequencies scaled by 0.9614 factor, the heat capacities ($C_{p,m}^{\theta}$), entropies (S_m^{θ}) and enthalpy changes (ΔH_m^{θ}) were calculated at different temperatures (Table 5). As seen from Table 5, the heat capacities ($C_{p,m}^{\theta}$), entropies (S_m^{θ}) and enthalpy changes (ΔH_m^{θ}) are gradually increased in the temperature range of 200–800 K due to the fact that the molecular vibrational intensities increase with temperatures. The empirical relations of the thermodynamic functions via temperatures were respectively fitted by quadratic, linear and quadratic formulas, and these corresponding fitting factors are all beyond 0.999, and the corresponding fitting equations are as follows:

$$C_{p,m}^{\theta} = -9.8812 + 1.4305T - 6.8 \times 10^{-4}T^2 \quad (7)$$

$$S_m^{\theta} = 335.34 + 1.0748T \quad (8)$$

$$\Delta H_m^{\theta} = -16.281 + 0.14475T + 3.78 \times 10^{-4}T^2 \quad (9)$$

3.5. Mulliken population analysis

The bonding capability of a molecule depends on the electronic charges on the chelating atoms. The atomic charge values were obtained by the calculation on the Mulliken atomic charges of the

studied molecule using B3LYP method with 6-31G(d) basis set. The atomic charge structure of DOIYAP is shown in Fig. 5. It is evident that the atomic charge populations are not evenly distributed in the whole molecule. Atoms N1, N2, N3, O1, O2, O3, C10 and C11 are negatively charged, while their directly bonded neighboring atoms (C1, C7, C9, C12 and C15) show obvious positive characteristics. As expected, the electrons in two benzene moieties of the studied molecule are in conjugation modes, while the charge populations are arranged in a positively–negatively staggered patterns in the middle part consisted of the pyrazoline and 2,5-dioxopyrrole moieties on the whole. The detailed Mulliken atomic charges except H atoms are listed in Table 6. The uneven charge distribution of the studied molecule is expected to present some interesting electron-transfer characteristics.

3.6. Frontier molecular orbitals

As we know that the frontier molecular orbitals (FMOs) play an important role in the electric and optical properties, such as, UV–vis absorption spectra and chemical reactions. Therefore, we examined the molecular orbital characteristics for the studied compound based on the optimized structure using GaussView 3.0 package [45]. Fig. 6 shows the distributions and energy levels of the FMOs computed at the B3LYP/6-31G(d) level for the studied molecule. As seen from Fig. 6, the atomic *p*-electron orbitals are responsible for the FMOs. The lowest unoccupied molecular orbital (LUMO) and LUMO + 1 are mainly localized on the dioxoisindoline fragment. The highest occupied molecular orbital (HOMO) and HOMO – 1 are localized on the antipyrine moiety. While the electrons of HOMO – 2 and HOMO – 3 mainly distribute in the phenyl ring. The energy levels of these higher occupied molecular orbitals are nearly close to each other agreeing within 1.171 eV. The small energy gap (LUMO–HOMO) is 3.639 eV, which indicates that the studied compound has high excitation energies.

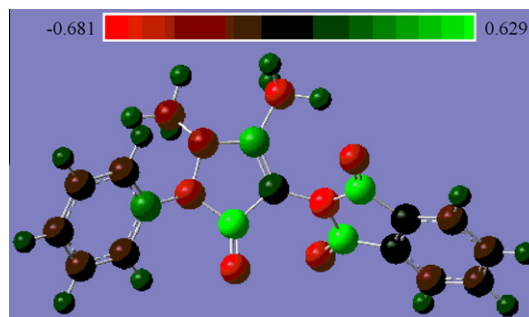


Fig. 5. The Mulliken charge distribution of DOIYAP.

Table 5
Thermodynamic properties of DOIYAP at different temperatures. ^a

T	$C_{p,m}^{\theta}$	S_m^{θ}	ΔH_m^{θ}
200.0	251.48	535.17	29.23
298.1	356.11	655.07	59.05
400.0	457.22	774.19	100.58
500.0	540.34	885.46	150.6
600.0	607.27	990.11	208.11
700.0	661.03	1087.91	271.62
800.0	704.7	1179.12	339.98

^a Temperatures (*T*) are in K; standard heat capacities ($C_{p,m}^{\theta}$) are in $\text{J mol}^{-1}\text{ K}^{-1}$; standard entropies (S_m^{θ}) are in $\text{J mol}^{-1}\text{ K}^{-1}$; standard enthalpy changes (ΔH_m^{θ}) are in kJ/mol .

Table 6
The Mulliken atomic charges of DOIYAP.

Atoms	Charges (e)	Atoms	Charges (e)
N1	-0.43925	C8	0.10220
N2	-0.34685	C9	0.40731
N3	-0.68117	C10	-0.52833
O1	-0.52383	C11	-0.32026
O2	-0.46192	C12	0.59369
O3	-0.47872	C13	0.04185
C1	0.28343	C14	0.04647
C2	-0.13898	C15	0.57625
C3	-0.14532	C16	-0.18032
C4	-0.12235	C17	-0.12804
C5	-0.14360	C18	-0.12799
C6	-0.15895	C19	-0.17834
C7	0.62845		

3.7. Nonlinear optical properties

In this study, the non-linear optical values of the studied molecule were calculated by the B3LYP/6-31G(d) method using Gaussian 03W program and are listed in Table 7. The total static dipole moment (μ_0), polarizability (α_0) and first hyperpolarizability (β_0) calculated by Eqs. (3)–(5) are 1.5684 Debye, 33.6921 Å³ and 2.7835×10^{-30} cm⁵/esu, respectively. The β_0 value is seven times magnitude of urea ($\beta_{0,\text{urea}} = 3.7289 \times 10^{-31}$ cm⁵/esu obtained by the same method). The β_0 value of the studied compound is obvious greater than the one of the previous similar compound [37], which also proves that the β_0 value increases with the increase of the π -electron conjugated effect of molecule.

Many research works have indicated that the frontier molecular orbitals (FMOs) have significant effects on material NLO properties [49,58,68–71]. The previous findings for series of similar compounds have demonstrated that the nonlinear optical properties of a material are associated with its molecular FMOs. Generally, the lower the HOMO–LUMO energy gap (ΔE) always leads to the larger the β_0 value. To better understand the relationship between the first-order hyperpolarizability and energy gap of the studied molecule, we examined the molecular HOMO and LUMO generated via Gaussian 03W program (Fig. 6). As shown from the surfaces of HOMO and LUMO in Fig. 6, we can find that the FMOs are mainly composed of atomic *p*-electron orbitals. It means that the first-order hyperpolarizability is caused by the charge-transferring characteristics of its molecular FMOs. More importantly, the result also indicates the investigated compound may be a good nonlinear optical material candidate due to the *p*-electron characteristics of molecular FMOs (Fig. 6).

3.8. Intramolecular electron migration

In order to reveal the various second order interactions between the filled orbital of one subsystem and the vacant orbital of another subsystem for the studied molecule, the NBO calculation was also performed by using Gaussian 03W package at the DFT-B3LYP/6-31G(d) level. Table 8 gives the second-order perturbation energy values, $E_{ij}^{(2)}$ corresponding to interactions and the overlap integral of each orbital pair.

As seen from Table 8, strong interactions can be observed in each of the three conjugative moieties, viz., phenyl ring, pyrazolone and dioxoisindoline. In the phenyl ring, the electron-donating bonds of BD(2)C1–C6, BD(2)C2–C3 and BD(2)C4–C5 present strong interactions to their neighboring electron-accepting anti-bonds of BD*(2)C2–C3, BD*(2)C4–C5, BD*(2)C1–C6, BD*(2)C4–C5, BD*(2)C1–C6 and BD*(2)C2–C3 with the respective interaction energies of 76.10, 85.31, 90.08, 83.13, 83.34 and 86.60 kJ/mol, which clearly indicate the π -electron delocalization characteristics of phenyl group. In the pyrazolone fragment, one of strong resonances is from BD(2)C8–C9 to BD*(2)O1–C7 with interaction energy of 105.15 kJ/mol, which is ascribed to the π -electron delocalization of the propen-1-one substructure; the N1 and N2 atoms respectively adopt hybridized $sp^{17.05}$ and $sp^{6.17}$ modes, and their lone pairs LP(1) N1 and LP(1) N2 present the electron-transfer potentials of 172.75 and 108.08 kJ/mol to the neighbor BD*(2)O1–C7 and BD*(2)C8–C9, respectively; the LP(2)O1 gives the neighbor acceptors of BD*(1)C7–C8 and BD*(1)N1–C7 with respective energies of 82.63 and 136.29 kJ/mol. In the dioxoisindoline moiety, No. 4 ring also shows strong interactions between electron-donating bonds and electron-accepting anti-bonds (Table 8); the N3 atom adopts hybridized $sp^{99.99}$ mode and presents obvious electron-transfer potentials of 193.22 and 206.49 kJ/mol to its neighboring BD*(2)O2–C12 and BD*(2)O3–C15, respectively; and the O2 and O3 atoms also present hyperconjugations with their corresponding anti-bonds, i.e., the LP(2)O2 displays the stabilized

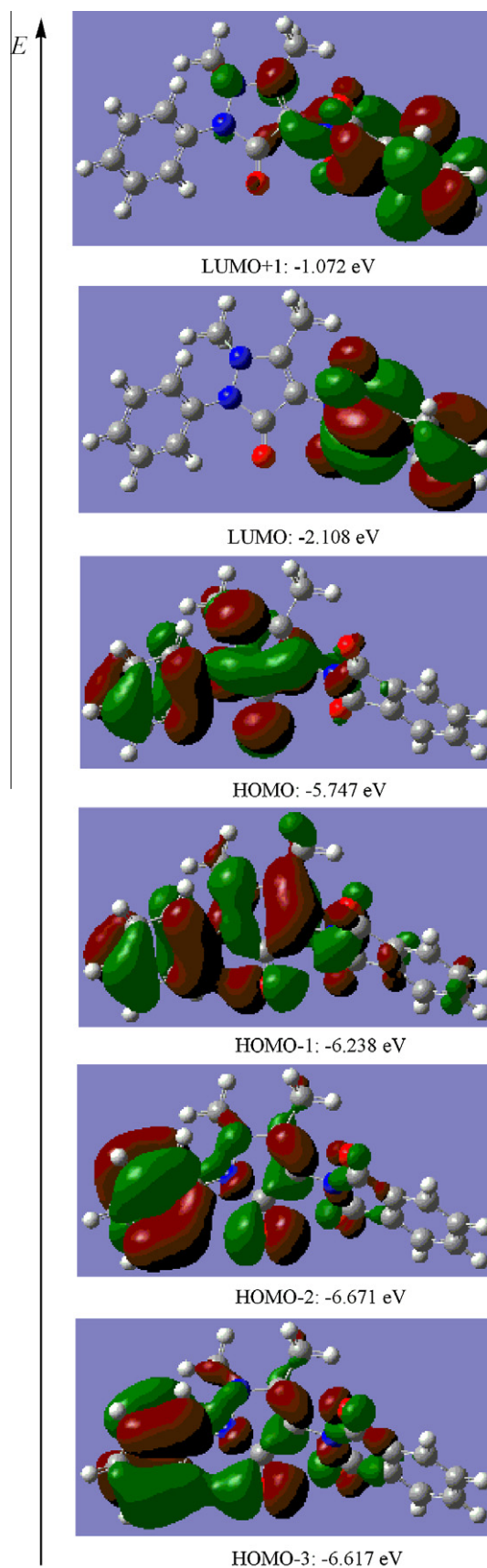


Fig. 6. Molecular orbital surfaces of selected FMOs of DOIYAP.

energies of 86.61 and 135.50 kJ/mol to BD*(1) C12–C13 and BD*(1) N3–C12, respectively, and the LP(2)O3 gives the respective

Table 7

The calculated dipole moments (Debye), static polarizability components (a.u.) and first-order hyperpolarizability components (a.u.) of DOIYAP.

μ_x	μ_y	μ_z	α_{xx}	α_{yy}	α_{zz}	β_{xxx}	β_{xxy}	β_{xyy}	β_{yyy}	β_{xzx}	β_{yyz}	β_{zxx}	β_{yzz}	β_{zzz}
0.343	1.514	-0.221	321.61	196.83	164.35	412.25	-62.03	-151.65	82.06	123.60	-63.74	52.70	44.60	-21.37

Table 8The second-order perturbation energies $E(2)$ (kJ/mol) corresponding to the most important charge transfer interactions (donor–acceptor) in DOIYAP calculated by B3LYP/6-31G(d) method. ^{a,b}

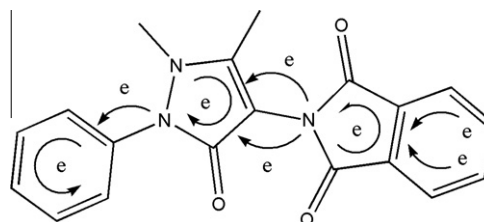
Donor(i)	ED(i) (e)	Acceptor(j)	ED(j) (e)	$E^{(2)}$ (kJ/mol)	$E(j) - E(i)$ (a.u.)	$F(i, j)$ (a.u.)
BD(2)C1–C6	1.6683	BD*(2)C2–C3	0.3177	76.10	0.30	0.066
BD(2)C1–C6	1.6683	BD*(2)C4–C5	0.3385	85.31	0.29	0.069
BD(2)C2–C3	1.6668	BD*(2)C1–C6	0.3930	90.08	0.27	0.069
BD(2)C2–C3	1.6668	BD*(2)C4–C5	0.3385	83.13	0.28	0.067
BD(2)C4–C5	1.6679	BD*(2)C1–C6	0.3930	83.34	0.27	0.067
BD(2)C4–C5	1.6679	BD*(2)C2–C3	0.3177	85.60	0.29	0.068
BD(2)C8–C9	1.8385	BD*(2)O1–C7	0.3624	105.15	0.31	0.083
LP(1) N1(sp ^{17.05})	1.6981	BD*(2)O1–C7	0.3624	172.75	0.31	0.103
LP(1) N2(sp ^{6.17})	1.7584	BD*(2)C8–C9	0.2588	108.08	0.36	0.086
LP(2) O1	1.8346	BD*(1)C7–C8	0.0764	82.63	0.70	0.107
LP(2) O1	1.8346	BD*(1)N1–C7	0.1071	136.29	0.63	0.130
BD(2)C13–C14	1.6240	BD*(2)C16–C17	0.3078	81.37	0.28	0.067
BD(2)C13–C14	1.6240	BD*(2)C18–C19	0.3068	80.41	0.28	0.067
BD(2)C16–C17	1.6265	BD*(2)C13–C14	0.4126	91.29	0.28	0.071
BD(2)C16–C17	1.6265	BD*(2)C18–C19	0.3068	82.42	0.28	0.067
BD(2)C18–C19	1.6240	BD*(2)C13–C14	0.4126	92.51	0.28	0.071
BD(2)C18–C19	1.6240	BD*(2)C16–C17	0.3078	82.67	0.28	0.067
BD(2)C13–C14	1.6240	BD*(2)O2–C12	0.2285	87.61	0.28	0.071
BD(2)C13–C14	1.6240	BD*(2)O3–C15	0.2424	92.38	0.27	0.072
LP(1) N3(sp ^{99.99})	1.6408	BD*(2)O2–C12	0.2285	193.22	0.28	0.104
LP(1) N3(sp ^{99.99})	1.6408	BD*(2)O3–C15	0.2424	206.49	0.27	0.106
LP(2) O2	1.8494	BD*(1)C12–C13	0.0725	86.61	0.68	0.108
LP(2) O2	1.8494	BD*(1)N3–C12	0.1035	135.50	0.65	0.131
LP(2) O3	1.8515	BD*(1)C14–C15	0.0718	85.18	0.69	0.108
LP(2) O3	1.8515	BD*(1)N3–C15	0.1033	132.19	0.65	0.130
LP(1) N1(sp ^{17.05})	1.6981	BD*(2)C1–C6	0.3930	78.90	0.31	0.070
BD*(2)C1–C6	0.3930	BD*(2)C2–C3	0.3177	901.05	0.01	0.081
LP(1) N3(sp ^{99.99})	1.6408	BD*(1)C7–C8	0.0764	31.35	0.73	0.071
LP(1) N3(sp ^{99.99})	1.6408	BD*(1)C8–C9	0.0269	20.43	0.88	0.064
LP(1) N3(sp ^{99.99})	1.6408	BD*(2)C8–C9	0.2588	24.11	0.30	0.038

^a ED, electron density; $E^{(2)}$, energy of hyperconjugative interactions; $\Delta\epsilon(i, j)$, energy difference between donor and acceptor i and j NBO orbitals; $F(i, j)$, the Fock matrix element between i and j NBO orbitals.

^b BD for 2-center bond, LP for 1-center valence lone pair, and BD* for 2-center antibond, the unstarred and starred labels corresponding to Lewis and non-Lewis NBOs, respectively.

stabilized energies of 85.18 and 132.19 kJ/mol to BD*(1) C14–C15 and BD*(1) N3–C15.

As expected, remarkable asymmetric interactions can be found between the three moieties of the studied molecule. Between the phenyl and pyrazolone moieties, the electrons of LP(1)N1(sp^{17.05}) can be redistributed into BD*(2)C1–C6 with the potential of 78.90 kJ/mol with external perturbations, then, the redistributed electrons of the BD*(2)C1–C6 can be easily transported to its neighboring anti-bond of BD*(2)C2–C3 with the higher interaction energies of 901.05 kJ/mol. Thus, the electrons of pyrazolone are transported into the phenyl ring of the molecule. Between the pyrazolone and dioxoisindoline moieties, the electrons of dioxoisindoline can be transported to pyrazolone substructure by transferring the electrons of the LP(1)N3 adopted sp^{99.99} hybridization to the anti-bonds of C7–C8 and C8–C9 with the total stabilized energy 75.89 kJ/mol. An interesting phenomenon can be found that the electron-transfer potentials are the same direction along with the molecular three moieties. Based on the NBO analysis of these data revealed by the second-order perturbation energies (Table 8), the intramolecular electron migration diagram can be obtained and illustrated in Scheme 2. The theoretical result indicates that the studied molecule has the long-range electron-transfer characteristics with external perturbation. It is remarkable that the electron-transfer direction obtained by the NBO analysis on the



Scheme 2. The electron-transfer potential diagram obtained by the NBO analysis for DOIYAP.

studied molecule is in accordance with the direction of electron transitions from the lower unoccupied molecular orbital to the higher occupied molecular orbitals, which indicates that the frontier molecular orbitals should be responsible for the long-range electron migration characteristics.

4. Conclusions

In this study, the title compound was synthesized in a one-step procedure and characterized by X-ray diffraction, spectroscopic techniques, as well as its thermodynamic, nonlinear optical and

electron-transfer properties have been obtained by the calculations at the DFT-B3LYP/6-31G(d) level using Gaussian 03W package.

From the structural parameters obtained by experimental XRD and theoretical optimization, most of the optimized bond lengths are slightly longer than the experimental values, and the optimized bond angles are slightly different from the experimental values. The vibrational spectra have been ascribed to the molecular structure with the help of the theoretical spectra. In the process of spectral assignment, the experimental and theoretical results are supported with each other, particularly, in the carbonyl vibrational assignments. The nonlinear optical calculation of studied molecule reveals that the first-order hyperpolarizability (β_0) of the compound is seven times as the value of urea. The NBO analysis result reveals that the studied molecule has long-range electron-transfer characteristics with external perturbations, and presents a long-range electron-transfer structural property with the energy gap of more than 3.639 eV when the orbital electrons are transported between the FMOs. The frontier molecular orbitals should be responsible for the NLO and long-range electron-transfer properties with external perturbations, such as, applied fields and suitable photon absorptions. The results indicate that the investigated compound may be an excellent photo-responsive material.

We hope the results are of assistance in the quest of experimental and theoretical evidences for the compound as reaction intermediates, spectral properties and photo-responsive materials.

Acknowledgements

This work was supported by Natural Science Foundations of China (Nos. 21073092 and 21103092) and Jiangsu Planned Project for Postdoctoral Research Funds (No. 1001011C). We also thank Qufu Normal University for Technical Assistance.

Appendix A. Supplementary material

Supplementary data associated with this article can be found, in the online version, at <http://dx.doi.org/10.1016/j.molstruc.2012.03.021>.

References

- [1] J.J. Li, Knorr Pyrazole Synthesis, Springer, Berlin, Heidelberg, New York, 2006, pp. 331–334.
- [2] E. Radzikowska, K. Onish, E. Chojak, Eur J Cancer 31 (1995) 225.
- [3] K.L. Khanduja, S.C. Dogra, S. Kaushal, R.R. Sharma, Biochem. Pharmacol. 33 (1984) 449.
- [4] I.D. Capel, M. Jenner, M.H. Pinnock, D.C. Williams, Biochem. Pharmacol. 27 (1978) 1413–1416.
- [5] S. Bondock, R. Rabie, H.A. Etman, A.A. Fadda, Eur. J. Med. Chem. 43 (2008) 2122.
- [6] S. Cunha, S.M. Oliveira, J.M. Rodrigues, R.M. Bastos, J. Ferrari, O.C. de, L. Kato, H.B. Napolitano, I. Vencato, C. Lariucci, J. Mol. Struct. 752 (2005) 32.
- [7] G. Plesch, M. Blahova, J. Kratsmar-Smogrovic, C. Friebe, Inorg. Chim. Acta 136 (1987) 117–121.
- [8] M.A. Madiha, A. Rania, H. Moatz, S. Samira, B. Sanaa, Eur. J. Pharmacol. 569 (2007) 222.
- [9] A.N. Evstropov, V.E. Yavorovskaya, E.S. Vorob, Z.P. Khudonogova, L.N. Gritsenko, E.V. Shmidt, S.G. Medvedeva, V.D. Filimonov, T.P. Prishchep, A.S. Saratikov, Pharm. Chem. J. 26 (1992) 426–430.
- [10] G. Turan-Zitouni, M. Sivaci, F.S. Kilic, K. Erol, Eur. J. Med. Chem. 36 (2001) 685–689.
- [11] T. Eicher, S. Hauptmann, The Chemistry of Heterocycles: Structures, Reactions, Synthesis and Applications, Wiley-VCH HmbH & Co. KGaA, 2003.
- [12] R.W. Boyd, The Nonlinear Optical Susceptibility, Academic Press, 2008.
- [13] H.M. Zeyada, M.M. El-Nahass, E.M. El-Menyawy, Solar Energy Mater Solar Cells 92 (2008) 1586–1592.
- [14] Y. Wang, Z. Yu, Y. Sun, Y. Wang, L. Lu, Spectrochim. Acta A 79 (2011) 1475–1482.
- [15] Y. Sun, Q. Hao, W. Tang, Y. Wang, X. Yang, L. Lu, X. Wang, Mater. Chem. Phys. 129 (2011) 217–222.
- [16] J.B. Foresman, A. Frisch, Exploring Chemistry with Electronic Structure Methods, Gaussian, Inc., Pittsburgh, USA, 1996.
- [17] C. Ravikumar, I.H. Joe, V.S. Jayakumar, Chem. Phys. Lett. 460 (2008) 552–558.
- [18] M. Kurt, T.R. Serbakan, M. Ozduran, Spectrochim. Acta A 70 (2008) 664–673.
- [19] Y. Sun, Q. Hao, W. Wei, Z. Yu, L. Lu, X. Wang, Y. Wang, J. Mol. Struct.: Theochem 904 (2009) 74–82.
- [20] Y. Sun, W. Wei, Q. Hao, L. Lu, X. Wang, Spectrochim. Acta A 73 (2009) 772–781.
- [21] Y. Sun, Q. Hao, W. Wei, Z. Yu, L. Lu, X. Wang, Y. Wang, J. Mol. Struct. 929 (2009) 10–21.
- [22] Y. Sun, Q. Hao, Z. Yu, W. Jiang, L. Lu, X. Wang, Spectrochim. Acta A 73 (2009) 892–901.
- [23] Y. Sun, Q. Hao, Z. Yu, W. Wei, L. Lu, X. Wang, Mol. Phys. 107 (2009) 223–235.
- [24] Y. Sun, Q. Hao, L. Lu, X. Wang, X. Yang, Spectrochim. Acta A 75 (2010) 203–211.
- [25] Y. Sun, Acta Crystallogr. E62 (2006) o5860–o5861.
- [26] Y. Sun, Chin. J. Struct. Chem. 26 (2007) 55–58.
- [27] Z. You, J. Wang, J. Chi, Acta Crystallogr. E62 (2006) o1652–o1653.
- [28] Y. Sun, D. Zhang, H. Song, Chin. J. Struct. Chem. 26 (2007) 511–514.
- [29] Y. Sun, R. Zhang, D. Ding, S. Liu, B. Wang, Y. Wang, Y. Lin, Struct. Chem. 17 (2006) 655–665.
- [30] R. Zhang, Y.X. Sun, Acta Crystallogr. E62 (2006) o5845–o5847.
- [31] Y. Sun, Acta Crystallogr. E62 (2006) o5858–o5859.
- [32] Y.F. Zheng, G.B. Yan, Y.B. Gu, Acta Crystallogr. E62 (2006) o5134–o5135.
- [33] Z. Jing, M. Yu, X. Chen, Q. Deng, Acta Crystallogr. E61 (2005) o3359–o3360.
- [34] T. Hökelek, M. Isiklan, Z. Kiliç, Acta Crystallogr. C57 (2001) 117–119.
- [35] Z.L. Jing, Z. Fan, M. Yu, X. Chen, C.H. Diao, Q.L. Deng, Acta Crystallogr. E61 (2005) o3532–o3533.
- [36] X.L. Zhang, Z.X. Li, Acta Crystallogr. E61 (2005) o266–o268.
- [37] G. Sun, Y. Sun, C. Yu, Z. Liu, C. Huang, L. Xu, J. Mol. Struct. 1006 (2011) 383–394.
- [38] J.L. Chambers, K.L. Smith, M.R. Pressprich, Z. Jin, SMART, Bruker Advanced X-ray Solutions, Version 5.628, Bruker AXS Inc., Madison, WI, 2002.
- [39] SAINTplus, Data Reduction and Correction Program, Version 6.22, Bruker AXS Inc., Madison, WI, 2001.
- [40] G.M. Sheldrick, SADABS, Program for Empirical Absorption Correction of Area Detector Data, University of Gottingen, Germany, 1996.
- [41] G.M. Sheldrick, SHELXS-97 and SHELXL-97; Programs for Structure Resolution and for Structure Refinement, University of Gottingen, Germany, 1997.
- [42] G.M. Sheldrick, SHELXTL, Structure Determination Software Suite, Version 6.10, Bruker AXS Inc., Madison, WI, 2000.
- [43] H. Arslan, Ö. Algül, T. Önkol, Spectrochim. Acta A 70 (2008) 606–614.
- [44] M.J. Frisch, G.W. Trucks, H.B. Schlegel, G.E. Scuseria, M.A. Robb, J.R. Cheeseman, J.A. Montgomery Jr, T. Vreven, K.N. Kudin, J.C. Burant, J.M. Millam, S.S. Iyengar, J. Tomasi, V. Barone, B. Mennucci, M. Cossi, G. Scalmani, N. Rega, G.A. Petersson, H. Nakatsuji, M. Hada, M. Ehara, K. Toyota, R. Fukuda, J. Hasegawa, M. Ishida, T. Nakajima, Y. Honda, O. Kitao, H. Nakai, M. Klene, X. Li, J.E. Knox, H.P. Hratchian, J.B. Cross, C. Adamo, J. Jaramillo, R. Gomperts, R.E. Stratmann, O. Yazyev, A.J. Austin, R. Cammi, C. Pomelli, J.W. Ochterski, P.Y. Ayala, K. Morokuma, G.A. Voth, P. Salvador, J.J. Dannenberg, V.G. Zakrzewski, S. Dapprich, A.D. Daniels, M.C. Strain, O. Farkas, D.K. Malick, A.D. Rabuck, K. Raghavachari, J.B. Foresman, J.V. Ortiz, Q. Cui, A.G. Baboul, S. Clifford, J. Cioslowski, B.B. Stefanov, G. Liu, A. Liashenko, P. Piskorz, I. Komaromi, R.L. Martin, D.J. Fox, T. Keith, M.A. Al-Laham, C.Y. Peng, A. Nanayakkara, M. Challacombe, P.M.W. Gill, B. Johnson, W. Chen, M.W. Wong, C. Gonzalez, J.A. Pople, Gaussian 03W, Version 6.0, Gaussian, Inc., Wallingford, CT, 2004.
- [45] R. Dennington II, T. Keith, J. Millam, K. Eppinnett, W. Lee Hovell, R. Gilliland, GaussView, Version 3.09, Semichem, Inc., Shawnee Mission, KS, 2003.
- [46] V. Krishnakumar, G. Keresztury, T. Sundius, R. Ramasamy, J. Mol. Struct. 702 (2004) 9–21.
- [47] P.L. Polavarapu, J. Phys. Chem. 94 (1990) 8106–8112.
- [48] A. Karakas, A. Elmali, H. Ünver, I. Svoboda, Spectrochim. Acta A 61 (2005) 2979–2987.
- [49] P.S. Liyanage, R.M. de Silva, K.M.N. de Silva, J. Mol. Struct.: Theochem 639 (2003) 195–201.
- [50] P.J. Mendes, J.P.P. Ramalho, A.J.E. Candeias, M.P. Robalo, M.H. Garcia, J. Mol. Struct.: Theochem 729 (2005) 109–113.
- [51] H. Alyar, Z. Kantarci, M. Bahat, E. Kasap, J. Mol. Struct. 2007 (2007) 516–520.
- [52] I.C. de Silva, R.M. de Silva, K.M. Nalin De Silva, J. Mol. Struct.: Theochem 728 (2005) 141–145.
- [53] J.O. Morley, J. Am. Chem. Soc. 110 (1988) 7660–7663.
- [54] H. Li, K. Han, X. Shen, Z. Lu, Z. Huang, W. Zhang, Z. Zhang, L. Bai, J. Mol. Struct.: Theochem 767 (2006) 113–118.
- [55] N. Sundaraganesan, J. Karpagam, S. Sebastian, J.P. Cornard, Spectrochim. Acta A 73 (2009) 11–19.
- [56] A.D. Tillekaratne, R.M. de Silva, K.M.N. de Silva, J. Mol. Struct.: Theochem 638 (2003) 169–176.
- [57] D. Sajan, H. Joe, V.S. Jayakumar, J. Zaleski, J. Mol. Struct. 785 (2006) 43–53.
- [58] K.S. Thanthirivatt, K.M. Nalin de Silva, J. Mol. Struct.: Theochem 617 (2002) 169–175.
- [59] A.E. Reed, L.A. Curtiss, F. Weinhold, Chem. Rev. 88 (1988) 899–926.
- [60] M. Amalanathan, V.K. Rastogi, I. Hubert Joe, M.A. Palafox, R. Tomar, Spectrochim. Acta A 78 (2011) 1437–1444.
- [61] M. Karabacak, M. Çinar, M. Kurt, J. Mol. Struct. 885 (2008) 28–35.
- [62] J.J. Meinel, A. Boudjada, A. Boucekkine, F. Boudjada, A. Moreac, S.F. Parker, J. Phys. Chem. A 112 (2008) 11124–11141.
- [63] A.P. Scott, L. Radom, J. Phys. Chem. 100 (1996) 16502–16513.

- [64] J.P. Merrick, D. Moran, L. Radom, *J. Phys. Chem. A* 111 (2007) 11683–11700.
- [65] J.S. Singh, *J. Mol. Struct.* 876 (2008) 127–133.
- [66] S. Sebastian, N. Sundaraganesan, B. Karthikeyan, V. Srinivasan, *Spectrochim. Acta A* 78 (2011) 590–600.
- [67] M. Amalanathan, I. Hubert Joe, V.K. Rastogi, *J. Mol. Struct.* 985 (2011) 48–56.
- [68] D.W.Y.L. Fei-Fei Li, *Polymer* 47 (2006) 1749–1754.
- [69] K. Oberg, A. Berglund, U. Edlund, B. Eliasson, *J. Chem. Inform. Comput. Sci.* 41 (2001) 811–814.
- [70] W. Zheng, N.B. Wong, W.K. Li, A. Tian, *J. Chem. Theory Comput.* 2 (2006) 808–814.
- [71] G. Tang, Z. Jiang, R. Li, J. Zhang, Y. Zhang, C. Zhang, *Spectrochim. Acta A* 74 (2009) 228–232.